Otoferlin Deficiency In Zebrafish Results In Defects In Balance And Hearing: Rescue Of The Balance And Hearing Phenotype With Full-length And Truncated Forms Of Mouse Otoferlin

Citation	Chatterjee, P., Padmanarayana, M., Abdullah, N., Holman, C. L., LaDu, J., Tanguay, R. L., & Johnson, C. P. (2015). Otoferlin Deficiency In Zebrafish Results In Defects In Balance And Hearing: Rescue Of The Balance And Hearing Phenotype With Full-length And Truncated Forms Of Mouse Otoferlin. Molecular and Cellular Biology, MCB.01439-14. doi:10.1128/MCB.01439-14
DOI	10.1128/MCB.01439-14
Publisher	American Society for Microbiology
Version	Accepted Manuscript
Terms of Use	http://cdss.library.oregonstate.edu/sa-termsofuse

Otoferlin Deficiency In Zebrafish Results In Defects In Balance And Hearing: Rescue Of The Balance And Hearing Phenotype With Full-length And Truncated Forms Of Mouse Otoferlin.

Paroma Chatterjee[1], Murugesh Padmanarayana[2], Nazish Abdullah[2], Chelsea L. Holman[2], Jane LaDu.[3], Robert L. Tanguay[1,3], Colin P. Johnson[1,2#].

1 Molecular and Cellular Biology program, 2 Dept. of Biochemistry and Biophysics, 3 Dept. Environmental and Molecular Toxicology, Oregon State University, Corvallis, Oregon 97331 phone: 541-737-4517

Correspondence should be addressed to Colin P. Johnson, Dept. Biochemistry and Biophysics, Oregon State University, Corvallis OR 97331 E-mail: colin.johnson@oregonstate.edu

Abbreviated title: Cross-species rescue of otoferlin in zebrafish

Number of Figures: 9

Conflict of Interest: The authors declare no competing financial interests.

Abstract

Sensory hair cells convert mechanical motion into chemical signals. Otoferlin, a six-C2 domain transmembrane protein linked to deafness in humans, is hypothesized to play a role in exocytosis at hair cell ribbon synapses. To date however, otoferlin has been studied almost exclusively in mouse models, and no rescue experiments have been reported. Here we describe the phenotype associated with morpholino induced otoferlin knockdown in zebrafish, and report the results of rescue experiments conducted with full length and truncated forms of otoferlin. We find that expression of otoferlin occurs early in development, and is restricted to hair cells and the midbrain. Immunofluorescence microscopy reveals localization to both apical and basolateral regions of hair cells. Knockdown of otoferlin results in hearing and balance defects, as well as locomotion deficiencies. Further, otoferlin morphants had uninflated swim bladders. Rescue experiments conducted with mouse otoferlin restored hearing, balance and inflation of the swim bladder. Remarkably, truncated forms of otoferlin retaining the C-terminal C2F domain also rescued the otoferlin knockdown phenotype, while the individual N-terminal C2A domain did not. We conclude that otoferlin plays an evolutionarily conserved role in vertebrate hearing, and that truncated forms of otoferlin can rescue hearing and balance.

Introduction

Hair cells couple mechanical motion to neurotransmitter release at synapses (21). In contrast to conventional neural synapses, hair cell synapses release neurotransmitter continuously and in a graded manner, (28) possess synaptic ribbons (7, 18, 28), and lack synaptophysin (10), complexin (25, 34-35, 43), Munc13 (46) and the calcium sensors synaptotagmin I and II (2). In place of synaptotagmin, it is believed that otoferlin may confer calcium sensitivity to evoke neurotransmitter release (15, 39). Otoferlin is a six-C2 domain transmembrane protein expressed in inner, outer, and vestibular hair cells, as well as restricted regions of the brain (39, 41, 47, 55). In humans, missense mutations in otoferlin have been linked to hearing loss (37, 54), and biochemical studies have determined that otoferlin binds calcium and lipids (15, 24), as well as membrane trafficking proteins (5, 11, 15, 32-33). Further, *in vitro* assays have demonstrated that otoferlin accelerates SNARE mediated membrane fusion (15). Based upon this evidence, it is hypothesized that otoferlin functions as a calcium sensitive regulator of neurotransmitter release in sensory hair cells.

However the results of several studies have raised questions related to otoferlin's function. For instance, despite otoferlin expression in vestibular hair cells, knockout mice show no balance defects (4, 42) despite reduced exocytosis in vestibular type I hair cells (48, 4). This raises questions as to the importance of otoferlin in this system. Further, otoferlin did not rescue synchronous neurotransmitter release in synaptotagmin I knockout cultured neurons, indicating that otoferlin and synaptotagmin are not functionally redundant (36). It is also unclear as to whether otoferlin related deafness can be rescued by introduction of a functional copy of the otoferlin gene, and no rescue

experiments have been reported. Related to this, it is currently unknown as to which domains of the protein are critical for hearing, and whether truncated otoferlin protein can recapitulate the function of wild-type otoferlin. To date, almost all studies on otoferlin have used a mouse model (20), and while insightful, current mammalian models present obstacles to progress in understanding otoferlin, including the challenge of hair cell isolation and difficulties in transfection. To circumvent such difficulties, and to add to the general body of knowledge of otoferlin across species, we have turned to zebrafish for the study of otoferlin. In this study we characterized otoferlin expression in zebrafish as well as the phenotype associated with knockdown. We also present rescue experiments using full-length and truncated forms of otoferlin.

Materials and methods

Fish strains.

Tropical 5D strains of zebrafish (*Danio rerio*) were used for this study and reared according to Institutional Animal Care and Use Committee protocols at the Sinnhuber Aquatic Research Laboratory, Oregon State University. Adult fish were raised on a recirculating water system (28 + 1°C) with a 14:10 hour light-dark schedule. Spawning and embryo collection were followed as described in (50).

Bioinformatic tools.

Protein sequences were obtained from Ensembl (Ensembl accession numbers: ENSP00000272371(human);ENSMUSP00000073803(mouse);ENSDARP00000123935 ,ENSDARP00000118166(zebrafish);ENSRNOP00000046997(rat);ENSOCUP00000013 417 (rabbit); ENSCPOP00000000288 (guinea pig); and ENSXETP00000007211 (Frog).

NCBI blastp tool was used to detect percent identity in the peptide sequences across different species with human as the query sequence. The blastp tool was further used to obtain percent identity across the different C2 domains of otoferlin keeping the human C2s as the query sequences. ClustalW and PRALINE tools were used for sequence alignments. SMART and SWISS-MODEL tools were used for domain analysis. R-software was used to create the dot-plot.

Real-time Quantitative Reverse Transcription Polymerase Chain Reaction (qPCR).

Total RNA was extracted from wild type (WT) embryos collected at different hours post fertilization (hpf) with RNAzol (Molecular Research Centre, OH, USA) and cDNA was synthesized using iScript cDNA synthesis kit (Bio-Rad, CA, USA). Gene-specific primers (Supplementary table A) were designed from genomic sequences for otoferlin b and otoferlin a found in Ensembl (Ensembl accession numbers: ENSDART00000149773 and ENSDART00000136255) and relative abundance assessed by qPCR performed using Power Sybr Green PCR master mix (Applied Biosystems, CA, USA). The data was normalized to otoferlin expression at 24 hpf for both isoforms. Also, the expression of myosinVIb (Ensembl accession number- ENSDART00000088801),vglut3 (Ensembl accession number- ENSDART00000080454) and sonic hedgehog a, shha (NCBI accession number – NM_131063.3) were examined in the otoferlin single and double KDs with gene-specific primers (Supplementary table A). The data was normalized relative to expression of the control and beta-actin genes. Graphs were plotted with the Prism software version 5.0.

Whole-mount Immunohistochemistry.

WT and microinjected zebrafish embryos were collected at different hpf and fixed in 4% paraformaldehyde overnight at 4°C. Mouse monoclonal anti-otoferlin and 3A10 (anti-Mauthner neurons) primary antibodies (dilution: 1:500, and 1:200, Developmental Studies Hybridoma Bank, University of Iowa, Iowa City, IA, USA) and rabbit polyclonal anti-myosinVI (dilution: 1:800, Proteus Biosciences, CA, USA) were used. AlexaFluor 488 and 555 goat anti-mouse (dilution: 1:1000, Molecular Probes, Invitrogen, Eugene, OR, USA) and AlexaFluor Goat anti-rabbit 594 (dilution: 1:500, Molecular Probes, Invitrogen, Eugene, OR, USA) secondary antibodies were used. Fixed embryos were washed with PBST and UltraPure distilled water (Invitrogen, CA, USA). Collagenase (0.0001g/ ml PBST, C9891; Sigma-Aldrich, MO, USA) treatment was performed to permeabilize the embryos, followed by rinsing with phosphate buffer saline. Permeabilized embryos were blocked with 10% normal goat serum (G6767; Sigma-Aldrich, MO, USA) for an hour and incubated with primary antibody overnight at 4°C. The following day samples were rinsed in phosphate buffer saline and incubated with secondary antibody. Embryos were imaged with an inverted Zeiss Axiovert 200M epifluorescence microscope fitted with a Zeiss Axiocam HRm camera and 5x objective.

Whole-mount *In Situ* Hybridization.

In situ hybridization (ISH) of otoferlin was performed with digoxygenin-labeled antisense RNA probes specific to zebrafish otoferlin a and otoferlin b on WT zebrafish embryos collected at different hpf as described in (45). Furthermore, ISH was performed as described in (45) with digoxygenin-labeled antisense RNA probes specific to the mouse otoferlin (NCBI accession number – NM_001100395.1) to detect expression of the hair-cell specific mouse otoferlin construct in larval zebrafish double morphants. To

synthesize the probe, gene-specific primers (Supplementary table B) with RNA polymerase promoter were designed for amplifying the probe templates, and cDNA was prepared from RNA isolated as described from whole zebrafish at 48 hpf. Embryos were labeled with either Fast Red (29) or NBT/BCIP stain. Stained embryos were imaged using an inverted Zeiss Axiovert 200M epi-fluorescence microscope and Nikon SMZ 1500 stereomicroscope mounted with a Coolpix E500 digital camera for NBT/BCIP.

In Situ Hybridization on larval zebrafish paraffin sections.

WT 120 hpf larval zebrafish were fixed in 10% neutral buffer formalin overnight at 4°C. The fish was rinsed in phosphate buffer saline and dehydrated in graded ethanol. Agar blocks were prepared using zebrafish metal molds (40) and pre-fixed zebrafish were arranged in the agar blocks. The agar blocks were sent to the Veterinary Diagnostic Lab, Oregon State University, Corvallis, OR for paraffin embedding and sectioning. Five micrometer sections were obtained and these sections were used for *in situ* hybridization (ISH) with digoxygenin-labeled antisense RNA probes specific to otoferlin a as described in (14, 45).

Plasmids and constructs.

The cDNA encoding mouse otoferlin was a gift from Christine Petit (Institut Pasteur, Paris, France). The *p5E-pmyo6b* vector used in cloning was a gift from Teresa Nicolson (Oregon health and Science University, OR, USA). The *p5E-pmyo6b* vector contains hair cell specific promoter for myosin VIb. Full length (FL) and truncated constructs of otoferlin were cloned downstream to the promoter at SacII and NotI sites. Clones were screened by colony PCR and verified by sequencing.

Microinjections.

A pair of morpholinos (MOs) targeting exon/intron boundaries of otoferlin a and otoferlin b and a standard negative control was obtained from GeneTools, Philomath, OR, USA (Supplementary table D). Approximately 2nl of 0.6 mM of otoferlin a MO, 0.7 mM of otoferlin b MO and both MOs diluted with RNAse-free ultrapure distilled water and 3% phenol red were pressure-injected in WT embryos at one-cell stage. For verification of splicing pattern and efficacy of knockdown, total RNA was extracted and cDNA was synthesized from injected and WT zebrafish embryos collected at different hpf as described. Gene-specific primers (Supplementary table E) were used for PCR with KOD Hot Start DNA Polymerase (Novagen, USA) and the products were separated on a 1.25% agarose gel.

For the rescue, approximately 600 pg of the vector construct with either mouse full-length (FL) otoferlin or truncated mouse otoferlin (construct with mouse putative C2DEF domains with the transmembrane, C2F domain with the transmembrane, C2EF domains with the transmembrane and C2A) were co-injected with the morpholinos. Capped RNA was synthesized with the mMessage mMachine transcription kit (Ambion, TX, USA) and PCR template. PCR template was amplified from pcDNA3 vector with the coding region for mouse full-length otoferlin using primers containing a T7-RNA polymerase promoter site. The amplified PCR template was purified with QIAquick PCR purification kit (Qiagen, CA, USA). Approximately 250 pg of synthesized mRNA were co-injected with the morpholinos. Larvae were screened for rescue of the balance phenotype, acoustic startle response including rescue of un-inflated swim bladder for further analysis.

Staining with vital dyes.

FM1-43FX dye (Life Technologies, NY, USA) labeling of neuromast hair cells was performed on live zebrafish at 120 hpf. Zebrafish larvae were immersed in 3 uM of FM1-43FX dye in embryo medium and rinsed off. The fish were washed several times with embryo medium and anaesthetized with 0.2 mg/ml tricaine solution for confocal imaging.

YO-PRO-1 (Life Technologies, NY, USA) staining of the neuromast hair cells was performed on live morpholino injected fish at 120 hpf. Zebrafish larvae were incubated for an hour at 28 deg C in 2uM YO-PRO-1 dye in embryo medium. The fish were washed three times with the embryo medium and anaesthetized with 0.2mg/ml tricaine solution for imaging with the inverted Zeiss Axiovert 200M epifluorescence microscope fitted with a Zeiss Axiocam HRm camera and 5x, 10x, 20x objectives.

Confocal image acquisition and processing.

Whole-mount immunohistochemistry preparations were mounted with 1% agar on 35 mm glass-bottomed petri dish and imaged with a confocal laser-scanning microscope fitted with a 40x oil-immersion objective (Zeiss LSM 510 Meta) with Alexa-Fluor 555 filter sets. For live zebrafish stained with vital dye FM1-43, fish were immobilized with 1% agarose containing 0.2 mg/ml tricaine on glass-bottomed petri dish and imaged with a 63x water-immersion objective (Zeiss LSM 510 Meta) with appropriate filter sets. Stacks of confocal images were taken and reconstructed with ImageJ software.

Larval behavior tests.

Injected zebrafish larvae were tested in a 96-well plate with the Viewpoint Zebrabox (Viewpoint Life Sciences, Lyon, France). Locomotor activity was measured using the Viewpoint tracker by subjecting the larvae to alternate phases of light and dark. Behavioral differences between the different injected groups were determined by comparing the distance moved during the dark period. Briefly, 96 hpf zebrafish larvae were loaded in a 96-well plate at least 3 hours prior to the experiment to give them sufficient time to acclimatize. Larvae were subjected to alternate phases of light followed by dark and finally light during which Viewpoint tracker recorded fish movement from the individual wells. Raw data files obtained from the Viewpoint were processed using a python script and JMP software to average the total distance travelled during the dark phase for each group. Graphs were plotted and statistically analyzed with the Graphapad Prism software version 5.0.

Acoustic Startle Response.

Injected zebrafish larvae from different groups were subjected to a startle stimulus assay at 120 hpf. Larvae were individually placed on a 100 mm petri dish filled with embryo medium and startled with a push-solenoid that generated a sudden tap when activated. Movement was recorded with a digital video camera (Sony,HDR CX22) for 30 secs after startling. The distance moved from the point of origin by different groups of larvae were compared by analyzing the video outputs from the camera with Noldus EthoVision XT(version 8.5) tracking software. Graphs were plotted and statistically analyzed with the Graphapad Prism software version 5.0.

Results

Zebrafish have two copies of otoferlin:

Contrary to mammals, the zebrafish genome contains two copies of otoferlin, located on chromosomes 17 and 20. The transcript (~8 kb) encoded by chromosome 17 will be referred to as otoferlin b with otoferlin a referring to the transcript encoded by chromosome 20 (~7 kb). A comparative study between the human otoferlin amino acid sequence with sequences from other species indicates that otoferlin is highly conserved (Figure 1A, B). Overall, the zebrafish otoferlin isoforms show 74% (otoferlin b) and 76% (otoferlin a) identity with human otoferlin (Figure 1B). Even higher identity was found when the comparison was restricted to sequences predicted to form C2 domains (Figure 1A). Comparison of the sequence identity between zebrafish otoferlin a and human otoferlin is 77% in the C2A domain, 91% in the C2B domain, 89% in C2C, 83% in C2D, 92% in C2E and 95% in C2F. Zebrafish otoferlin b is 91% similar in the C2B, 89% in the C2C, 83% in C2D, 88% in C2E, and 94% in C2F domains with human otoferlin. Zebrafish otoferlin a appears to be a closer representation of the human otoferlin because of the presence of all six C2 domains unlike otoferlin b that lacks the C2A domain (Figure 1A, Figure 1C). The identity between amino acid sequences of the two zebrafish otoferlin isoforms is ~80%. From the diagonal in the center of the dot-plot (Figure 1D) it can be discerned that the zebrafish otoferlin peptide sequences are identical in most regions except in the first ~200 amino acids. On further comparison by sequence alignments (data not shown) it was confirmed that the peptide sequence of otoferlin b was ~180 amino acids shorter on the N-terminal than otoferlin a. In summary, the sequences of the C2 domains are more conserved than the non-C2 domain regions, and the C2A domain is the least conserved of the C2 domains.

Otoferlin expression and localization in zebrafish:

The amino acid sequence of otoferlin is similar across species including zebrafish, suggesting a conserved function. Given the ease with which the organism can be genetically manipulated, we chose zebrafish as our model for use in the study of otoferlin. To ascertain the developmental expression profile of otoferlin we conducted qPCR on wild-type (WT) zebrafish samples collected every 24 hours during the first 120 hours post fertilization (hpf). We found that 24 hpf zebrafish larvae express both copies of otoferlin (Figure 2A) with an increase in relative abundance of both transcripts at 48 hpf (Figure 2A). Expression plateaus after 72 hpf. The rise in otoferlin expression during the first 72 hours of embryonic development coincides with the deposition of neuromasts and formation of the aLL (anterior lateral line) and pLL (posterior lateral line). It also coincided with formation of the semicircular canals and otic vesicle occurring during this stage of development (19). We next sought to characterize the spatial pattern of otoferlin expression in zebrafish larvae using whole-mount *in situ* hybridization (Figure 2B). Transcripts of otoferlin b were detected in the otic placode of 24-hour old larvae (Figure 2B). The otic placode eventually forms sensory patches and develops as the zebrafish inner ear (49). There was also weak expression of otoferlin b in primordial cells that form neuromasts of the zebrafish lateral line organ system (Figure 2B). The expression of otoferlin b becomes pronounced in the neuromasts of pLL, aLL and the inner ear region as the zebrafish larvae continues to develop through 120 hpf (Figure 2B). Transcripts of otoferlin a were detected at around 24 hpf in the otic placode (Figure 2B) and is restricted to the sensory patches of the inner ear as the larvae continues to develop through 120 hpf (Figure 2B). We observed a relatively weak

and diffuse expression in the zebrafish brain region and in the retina starting at around 48 hpf that became prominent at 120 hpf (Figure 2C). Analyses of sectioned 120 hpf larval zebrafish confirmed expression of otoferlin transcripts in the mid-brain and the retinal ganglion cell layer (Supplementary Figure 1). However, no expression of the otoferlin a transcript was detected in the hair cells of the aLL and pLL neuromasts (Figure 2B).

Whole-mount immunohistochemistry on WT zebrafish larvae with the anti-otoferlin HCS-1 antibody was consistent with the mRNA expression profile in the inner ear and lateral line (Figure 2B) during the first 120 hours of zebrafish development (8). Strong immunoreactivity in the nascent hair cells of the zebrafish otic region at 24 hpf was detected (Figure 3A), and immunoreactivity is detectable in the hair cells of both the pLL and aLL at 48 hpf (Figure 3B) becoming more pronounced between 72-120 hpf (Figure 3C, D, F). Negative controls at 72 hpf (Figure 3E) with no primary antibody confirmed that the labeling observed is due only to binding of the secondary antibody to the HCS-1 antibody. Overall the onset and increase of otoferlin expression correlates with the formation and development of the zebrafish inner ear and the pLL and aLL system (19).

To examine the sub-cellular localization of otoferlin in zebrafish hair cells, confocal images of 120 hpf larvae were collected. Pronounced immunolabeling in both the supranuclear and basolateral compartments including a punctate distribution throughout the cytoplasm was observed in hair cells of the neuromast (Figure 3G). This subcellular distribution is similar to observations made on mouse hair cells (5, 31, 33). Probing 120 hour wild-type zebrafish with the FM1-43 dye (Figure 3H) showed uptake in

the apical end of the hair cells of a posterior lateral line neuromast cluster indicating active vesicle recycling (9). This overlap in otoferlin distribution and FM1-43 dye uptake in the apical hair cell compartment raises the possibility of another role of otoferlin in the apical region in addition to the established function in synaptic transmission at the basolateral region (31, 39). To validate expression of otoferlin in the zebrafish hair cells, dual immunofluorescence was performed on wild-type 120 hpf larval zebrafish with anti-otoferlin and anti-myosin VI antibodies. Myosin VI is a marker for hair cells, and fluorescence images confirm that otoferlin co-localizes with myosinVI in larval zebrafish hair cells (Figure 3I) (16, 38).

Knockdown of otoferlin in the zebrafish hair cells:

To determine the function of otoferlin *in vivo,* we used anti-sense splice-blocking morpholinos that targeted both isoforms including their splice variants. Two splice-blocking MOs for each otoferlin gene targeting exon-intron boundaries (otoferlin b MOs– e2i2 and e38i38; otoferlin a MOs- i6e7, e11i11) (Figure 4A) were designed and microinjected at the one–cell stage. Comparable phenotypes were observed with each pair of morpholinos, and the e38i38 MO targeting otoferlin b, and i6e7 MO targeting otoferlin a were used for subsequent experiments in this study. We evaluated mRNA expression to assess knockdown of the otoferlin a and b transcripts in the single and double morphants. Analysis of qPCR data indicates that the expression of otoferlin a is significantly reduced in the otoferlin a and otoferlin b+a KD groups (p-value <0.001) (Figure 4D). Similarly, otoferlin b is significantly reduced in the otoferlin b and otoferlin b+a KD groups (p-value <0.001) (Figure 4D). RT-PCR further supports the conclusion that both the single and double knockdowns were effective at 96 hpf (Figure 4B; lanes

4, 5, 6 and 7) when compared with age-matched microinjected controls (Figure 4C, lanes 1 and 2) and lasted up to 120 hpf (Supplemental Figure 2A). As the otoferlin b and a sequences are ~80% identical (Figure 1C), it was necessary to validate the specificity of MOs that were designed to target each isoform separately. Analysis of qPCR data indicates that knockdown of otoferlin b does not significantly affect the expression of otoferlin a and vice versa (Figure 4D). RT-PCR further supports the conclusion that each MOs specifically block the targeted otoferlin without affecting expression of the other isoform at up to 120 hpf (Figure 4C and Supplemental Figure2B).

Since otoferlin interacts with the hair cell marker myosinVI (38, 11), and a reduction in otoferlin decreases the immunofluorescence of synaptic vesicle marker VGlut3 (31), qPCR was conducted on otoferlin single and double morphants to measure the relative expression changes of both myosin VI and VGlut3. Analysis indicates that otoferlin knockdown does not significantly affect the expression of myosin VI or VGlut3 in larval zebrafish at 96 hpf (Figure 4D).

Immunohistochemistry on 120 hpf injected control (Figure 5A) and morphant larvae (Figure 5B-D) was also conducted. Embryos injected with the otoferlin b morpholino show staining in the hair cells of the inner ear (Figure 5B). However, there was no detectable signal in the hair cells of the neuromasts of the pLL and aLL (Figure 5B). Contrary to otoferlin b, the otoferlin a morphants show staining in the hair cells of the inner ear with strong immunolabeling in the hair cells of the neuromasts of pLL and aLL (Figure 5C). Visual inspection of the otic region reveals that in comparison to the control zebrafish larvae (Figure 5E), otoferlin a is distributed in the hair cells of the

sensory patches of the anterior macula. It is also present in the hair cells of the posterior, anterior and medial cristae (Figure 5F). However, otoferlin b is distributed in hair cells of the sensory patches of both the anterior and posterior maculae but absent from the cristae (Figure 5G). This suggests that the otoferlin isoforms might play distinctive roles in the otic region. Finally, otoferlin b and a double morphants show no anti-otoferlin signal in any of the sensory patches of the inner ear and neuromasts of the lateral line (Figure 5D). Confocal microscopy images of immunolabeled 120 hpf injected controls and double morphants were also collected (Supplementary Figure 3A and 3B). In contrast to control siblings, a compressed z-stack image of the head region of double morphants showed absence of anti-otoferlin in the otic region. This indicates a complete knockdown of both isoforms of the zebrafish otoferlin in the otoferlin b+a double morphants to the limits of detection.

Phenotypic analysis of the otoferlin single and double knockdowns:

Compared to age-matched injected controls (Figure 6A), otoferlin single knockdowns show no noticeable defects in gross morphology at 120 hpf (Figure 6B and C). However, after 96 hpf the double morphants fail to develop an inflated swim bladder (Figure 6D) compared to single knockdowns and injected controls. The phenotypic defects are visible around 72 hpf in the double morphants when they fail to maintain an upright position compared to injected control siblings (Figure 6E and F). This suggests a balance defect (27) and indicates a critical contribution of otoferlin to balance and vestibular function. Moreover about 80% of the the 96 and 120 hour double morphants swim on their sides or back, land head-on and often float vertically with head-up. On touching with a hair, double KDs exhibit a circling and looping motion (Supplementary

movie 1 and 2), but swim back to the source of the stimulus rather than escaping. Beyond 120 hpf, double morphants gradually develop a curved spine compared to injected controls (Figure 6G and H) that enhances the circling movement. These phenotypic abnormalities are comparable to the 'circler mutants' (16, 27, 30) that were determined to be mutations in sensory hair cell related genes. Since we observed a defective escape response with the double morphants, we examined the morphological differences in the patterning of the lateral line with hair cell marker YO-PRO-1. We did not observe differences in staining between the control and otoferlin b+a double morphants (Figure 7A). Further, bright-field images of the otic region indicate that, compared to controls, the semicircular canal folds and otolith form normally in 120 hpf otoferlin double morphants (Figure 7B). A similar swim bladder phenotype was observed in the double morphants that had been injected with a second set of morpholinos, e11i11 - otoferlin a and e2i2- otoferlin b (Supplementary Figure 4A).

Given that the double morphants show an uninflated swim bladder phenotype we tested whether otoferlin knockdown affected swim bladder development using qPCR analysis of shha in double morphants at 72 hpf. shha is a swim bladder developmental marker (51) , and results indicate that relative to control, the expression level of the shha gene does not change in the double morphants (Supplementary Figure 4B).

Since both isoforms of otoferlin are expressed in hair cells of the otic region and lateral line, both copies may play a role in hearing and balance. To test whether otoferlin knockdown impairs hearing, acoustic startle reflex assays were conducted on 120 hpf single and double morphants. Acoustic startle assays are widely used to evaluate hearing induced escape response in larval zebrafish (27). As shown in Figure

8C, the distance travelled by control larvae (n=23) was 63.94 mm, while otoferlin b KD (n=18) was 66.03 mm and otoferlin a KD (n=17) was 66.79 mm. When the single KDs were compared to control using Dunn's multiple comparison with standard 5% significance level, the test showed no significant difference. By contrast, double KDs (n= 16) travelled only 22.92 mm after startling. This value is significantly lower (Dunn's multiple comparison, p-value < 0.001) when compared with the distance moved by the single KD and age-matched controls. A summary comparing the startle between otoferlin single and double morphants as well as the control group is included in Supplementary Figure 5. These results suggest that there is redundancy of function between the two isoforms and the startle escape is significantly attenuated when expression of both the isoforms are reduced. To ensure that the larval zebrafish movement is not random but coincides with the startle stimuli the average startle velocity as a function of time was plotted. The movement of the larval fish coincided with the startle stimuli for both the control and the double morphants (Figure 8D). Furthermore, the control fish show a marked increase in velocity after startling followed by a decrease, while the double morphants show some slight movement after startling which quickly declines relative to control (Figure 8D). This data is consistent with the defective escape response observed in the double morphants when compared to age-matched controls.

Studies on mouse models have established a link between otovestibular defects and locomotion using a dark-light test (17, 22). Upon finding that zebrafish otoferlin morphants exhibit balance defects and an abnormal startle escape response, dark-light locomotory tests were conducted on control and KD larval fish. 96 hpf otoferlin single

Molecular and Cellular Biology

(n=72) and double (n=72) morphants, as well as age-matched controls (n=72) were used for the dark-light assay. Compared to controls, single KD traveled less during the dark phase (Mean distance travelled; control = 62.73 mm, otoferlin b KD= 45.67mm, otoferlin a KD = 46.68 mm; Dunn's multiple comparison test, p-value <0.05) (Supplementary Figure 6), and double KD fish travel even less (otoferlin double KD = 35.61 mm; Dunn's multiple comparison test, p-value <0.001) (Supplementary Figure 6). Since the zebrafish single and double morphants shows a defective dark-light response, this might indicate a direct or indirect role of otoferlin on neuronal wiring in the larval zebrafish. However, comparison of immunofluorescently labeled Mauthner cells that mediate the escape response (3, 6, 56), did not reveal any gross defects in the double morphants (n=3) as compared to age-matched controls (n=2) (Supplemental Figure 5E and F).

Rescue of zebrafish otoferlin knockdown with mouse otoferlin:

From comparison it is evident that there is a high sequence similarity between otoferlin of different species, suggesting functional conservation (Figure 1A and B). To test for functional conservation we co-injected double morphants with a *p5E-pmyo6b* vector encoding mouse otoferlin and a hair cell specific myosin VIb promoter, and tested for rescue of the knockdown phenotype. Several constructs including the full length mouse otoferlin (FL-otoferlin), as well as truncated forms of the protein were used in this study to identify the domain(s) critical for otoferlin function (Figure 8A). Expression of mouse otoferlin was validated by performing whole-mount immunohistochemistry on zebrafish double morphants co-injected with the FL-otoferlin construct. Figure 8B shows that the expression of the FL-otoferlin construct is restricted only in the hair cells of the otic

region and the lateral line thereby confirming that the myosin VIb promoter recapitulates endogenous otoferlin expression. We also performed whole mount *in situ* hybridization experiments on zebrafish double morphants co-injected with the mouse FL-otoferlin construct. Supplementary Figure 5A, B, and C shows the presence of otoferlin transcripts in the otic region, pLL, and aLL. Figures 8C, 8D and Supplementary Figure 6 show that the FL-otoferlin was able to rescue the startle escape response (mean distance moved =59.58 mm, n= 18, no significant difference with control group in Dunn's multiple comparison test with standard 5% significance level) and dark-light behavior in the zebrafish double morphants (mean distance travelled during dark-phase = 59.89 mm, n=72, no significant difference with control group in Dunn's multiple comparison test with standard 5% significance level). Mouse FL-otoferlin also rescues the swim bladder defects observed in 120 hpf zebrafish double morphants (Figure 9A). Furthermore, FM1-43 uptake in the rescue larvae was indistinguishable from WT larvae (data not shown). These results suggest that the mouse otoferlin was sufficient to correct for the disorders associated with depletion of both otoferlin isoforms found in larval zebrafish.

Remarkably, we were able to rescue the double morphants with a truncated form of mouse otoferlin lacking the first three putative C2 domains (ΔABC). Zebrafish double morphants co-injected with the ΔABC construct were found to have inflated swim bladders as observed at 120 hpf (Figure 9B). The startle reflex abnormalities (Figures 8C and 8D) were also rescued (mean distance moved =63.32 mm, n=19, no significant difference with control group in Dunn's multiple comparison test with standard 5% significance level). In addition, dark-light behavior was also rescued (mean distance

travelled during dark-phase = 59.81 mm, n=48, no significant difference with control group in Dunn's multiple comparison test with standard 5% significance level) (Supplementary Figure 6). This suggests that the first three C2 domains are not required to correct for the balance and hearing deficits that were observed with the zebrafish double morphants.

Several additional truncated constructs (Figure 8A) lacking either the first 4 or 5 C2 domains (Δ-ABCD, Δ-ABCDE) or consisting of only the N-terminal C2A domain (Δ-BCDEF) were also tested for recovery of the uninflated swim bladder (Supplementary Figure 7A and 7B) and acoustic startle response (Figure 8C). The ΔABCD (n = 25, mean distance = 53.94 mm) and ΔABCDE (n = 23, mean distance = 52.00 mm) displayed no significant difference relative to the control group in Dunn's multiple comparison test with standard 5% significance level (Figure 8C). Co-injection of the double morphants with the ΔBCDEF construct did not rescue the acoustic startle responses however (n = 16, mean distance = 26.57 mm, no significant difference with otoferlin b+a KD group in Dunn's multiple comparison test with standard 5% significance level) (Figure 8C).

Finally, as an alternative method of rescue, zebrafish double morphants were co-injected with mouse otoferlin mRNA encoding the full-length protein. The mRNA injection completely rescued the swim bladder defect (Figure 9C) including recovery of the startle escape response (mean distance moved = 65.55 mm, n = 17, no significant difference with control group in Dunn's multiple comparison test with standard 5% significance level), (Figure 8C) supporting the conclusion that mouse otoferlin can rescue morpholino knockdown in zebrafish. A table showing percentage of larvae with

472 inflated swim bladder rescue phenotype for the double morphants co-injected with the
473 different otoferlin constructs is included in Figure 9D.

474 **Discussion**

475 Based upon sequence, expression patterns, knockout phenotype, as well as rescue
476 studies, we conclude that otoferlin plays a conserved role in hair cells. Despite
477 divergence of the zebrafish and mammalian genomes approximately 420 million years
478 ago (13), the amino acid sequences of otoferlin are highly similar, and mouse otoferlin
479 successfully compensates for loss of endogenous otoferlin expression in zebrafish. This
480 suggests both a conserved function of the protein in hair cells, and a conserved set of
481 binding partners for neurotransmitter release. Indeed, the loss in hearing we observed
482 in otoferlin knockdown zebrafish matches mouse knockout models. We also note that
483 while zebrafish have two otoferlin genes and mammals have one, multiple splice
484 isoforms of the gene have been reported for mice and humans (33, 53).

485 Analysis of sequence identity of the C2 domains between species show greater
486 conservation among the C-terminal C2D, C2E, and C2F domains compared to the N-
487 terminal C2A domain. We speculate that these C-terminal domains may play a
488 functionally conserved or redundant role in otoferlin function. Indeed, functional
489 redundancy among the C2 domains has been noted in reconstituted membrane fusion
490 assays (15). Experiments we report indicate that shortened forms of otoferlin lacking the
491 N-terminal domains rescue the knockdown phenotype, in agreement with the idea of
492 functional redundancy. However it is possible that the N-terminal C2 domains play a

role that was not detected in our assays or a function found in mammals but not in zebrafish. Indeed, our results seem to conflict with reports of missense mutations in the C2B and C2C domains that have been linked to hearing loss in mammals (23,26) We speculate that these missense mutations may reduce the structural stability of the protein, resulting in lower levels of protein expression. Knockdown of both zebrafish otoferlin genes was required for an observable phenotype in our studies, despite differing in the first N-terminal 183 amino acids, corresponding to the C2A domain, again suggesting that some domains may be dispensable. Interestingly, biophysical studies on the C2A domain have determined that this is the only domain in otoferlin that does not bind calcium (12,15). However, studies on the otoferlin orthologues myoferlin and dysferlin have found that the C2A domain of these proteins do bind calcium, supporting the idea that the calcium binding activity of the C2A domain may have diverged among the ferlins (1, 15, 24, 44).

Unexpectedly, otoferlin knockdown zebrafish displayed severe deficits in balance and uninflated swim bladders, suggesting a critical role for otoferlin in balance. While expressed in vertebrate vestibular hair cells, neither otoferlin knockout mice nor human patients with otoferlin mutations suffer from balance deficits (4). Our results clearly demonstrate a critical role for otoferlin in zebrafish balance and vestibular hair cell function. That calcium dependent neurotransmitter release is attenuated but not completely abrogated in knockout mouse vestibular hair cells (4) may indicate that compensatory or redundant calcium sensors exist in mammalian hair cells that are not active in zebrafish cells. Thus zebrafish may serve as a model for future characterization of otoferlin's contribution to vestibular hair cells.

Despite the loss of morpholino knockdown efficiency and expression of both otoferlin genes around 120 hpf, most zebrafish did not show any signs of swim bladder inflation or recovery of balance even at 10 dpf, and many developed a curved spine. This suggests that otoferlin may play a developmental role, and that the lack of otoferlin during a certain developmental window may have permanent effects on zebrafish physiology. In support of this, a recent study reported abnormally small ventral cochlear nuclei in otoferlin knockout mice (52). Future studies should focus on the developmental effects linked to otoferlin loss-of-function.

Figure Legends:

Figure 1 - Sequence identity of otoferlin across different species. A) Percent dentity of predicted otoferlin C2 domains of various species compared to human otoferlin. **B)** Comparison of overall sequence identity of otoferlin with human otoferlin. **C)** Zebrafish otoferlin isoforms with putative C2 domains. Otoferlin b lacks the C2A domain. **D)** Dot-plot showing the identity of amino acid sequence between the two zebrafish otoferlin proteins: otoferlin a and otoferlin b. The diagonal across the plot indicates highly identical sequnces. Breaks along the diagonal indicate regions which are non-identical. The asterisk (*) designates the absence of the C2A domain (amino acid = 3- 97).

Figure 2 – mRNA expression of otoferlin in developing zebrafish. **A)** Fold expression of otoferlin a and b transcripts at 24-120 hpf. Expression is normalized to 24 hpf. Error bars indicate 95% confidence interval of the sample mean (n=5). **B)** Whole-mount in situ hybridization images showing expression of otoferlin in 24-120 hpf wild-type zebrafish larvae. Upper panel – Expression of otoferlin b. Arrows indicate sensory patches in the

inner ear. Arrowheads indicate anterior and posterior lateral line neuromasts; Lower panel – Expression of otoferlin a. Arrows indicate sensory patches in the inner ear. **C)** Expression of otoferlin a in the brain region and retina in a 120 hpf zebrafish larvae. Arrows indicate brain and retina.

Figure 3 - Otoferlin protein expression in developing zebrafish. (A-F) Whole-mount immunohistochemistry on wild-type larval zebrafish at indicated developmental time points (24-120 hpf). **E)** Negative control with no primary antibody in 72 hpf wild-type larvae. White circles indicate the position of the eye, arrows indicate sensory patches of the ear, arrowheads denote anterior and lateral line neuromasts. **G)** Confocal image showing sub-cellular distribution of otoferlin in a 120 hpf hair cell neuromast cluster. Arrowhead indicates the supranuclear region of the hair cell, arrow indicates basolateral compartment of the hair cell (Scalebar 10um). **H)** Confocal image showing uptake of FM1-43 dye uptake in the apical end (arrowhead) of hair cells within a neuromast of the posterior lateral line. Dye incubation time – 3 minutes. **I)** Dual Immunofluorescence with wild-type 120 hpf zebrafish showing co-localization of otoferlin in the hair cells of the neuromast with another hair cell marker, myosinVI. White boxes 1 and 2 indicate regions of co-localization. Insets of region 1 and 2 showing otoferlin co-localizing with myosinVI.

Figure 4 - Morpholino knockdown of otoferlin in zebrafish larvae. A) Diagram of four splice-blocking morpholinos used in this study targeting otoferlin a and otoferlin b (e= exon; i= intron). **B)** RT-PCR gel image of otoferlin KD zebrafish larvae at 96 hpf, (lane 1) = molecular weight marker ; (lane 2) = negative control tested for otoferlin b; (lane 3) = negative control injected tested for otoferlin a; (lane 4)= otoferlin b KD tested

for otoferlin b; (lane 5) = otoferlin a KD tested for otoferlin a; (lane 6) = otoferlin b+a double KD tested for otoferlin b; (lane 7) = otoferlin b+a double KD tested for otoferlin a. **C)** Cross expression studies with 96 hpf zebrafish larvae. RT-PCR gel image shows expression of: (lane 1)= molecular weight marker; (lane 2) = otoferlin a in control; (lane 3)= otoferlin a in otoferlin b KD; (lane 4) = otoferlin b in otoferlin b KD; (lane 5) = otoferlin b in control; (lane 6)= otoferlin b in otoferlin a KD; (lane 7) = otoferlin a in otoferlin a KD. (Inj. C – injected control, KD – Knockdown, otof a – otoferlin a, otof b – otoferlin b, otof b+a – otoferlin b+a) **D)** qPCR bar graph showing relative expression of otoferlin a, otoferlin b, myosinVI and VGlut3 genes in 96 hpf larval zebrafish across control, otoferlin a KD, otoferlin b KD and otoferlin b+a KD groups where each gene is normalized with respect to the corresponding controls. For the Myosin VI and Vglut3 genes, no statistical deviation in expression is observed among the different KD groups. Expression of otoferlin a is significantly reduced (p value <0.001) in the otoferlin a and otoferlin b+a KD groups, but not in the otoferlin b KD. Otoferlin b expression is significantly reduced in the otoferlin b and otoferlin b+a KD groups (p value <0.001), but not in the otoferlin a KD. The statistical significance is calculated through Bonferroni multiple comparisons in prism software. Error bars indicate 95% confidence interval of the sample mean (n=3).

Figure 5 - Whole mount immunohistochemistry with the HCS-1 anti-otoferlin antibody. A) 120 hpf larvae showing otoferlin expression in control injected, **B)** otoferlin b KD, **C)** otoferlin a KD, **D)** otoferlin b+a KD. Fluorescent MIP (maximum intensity projection) image of **E)** Injected Control, **F)** Otoferlin b KD, **G)** Otoferlin a KD, of 120 hpf larval otic region showing distinct distribution of otoferlin in the sensory patches of

cristae and maculae (ac, anterior crista; mc, medial crista; pc, posterior crista; pm, posterior macula; am, anterior macula).

Figure 6 - **Observable phenotypes associated with the otoferlin KD 120 hpf larval zebrafish. A)** Control injected, **B)** otoferlin b KD, **C)** otoferlin a KD, **D)** otoferlin b+a double KD (arrows denote the swim bladder). The otoferlin double KDs fail to develop an inflated swim bladder. **E)** 72 hpf control larvae maintains an upright posture, **F)** 72 hpf otoferlin b+a double KDs fail to maintain an upright posture **G)** 10-day old injected control larvae, **H)** 10-day old otoferlin b+a double KD zebrafish fail to inflate their swim bladders (arrow) and develops a curved spine (arrow-head).

Figure 7 - **Otoferlin KD effect on structure and formation of lateral line, otic vesicle and semicircular canals. A)** (upper panel) Yo-Pro1 uptake in injected control larval zebrafish at 120 hpf, (lower panel) Yo-Pro1 uptake in otoferlin b+a double KD larval zebrafish at 120 hpf **B)** (upper panel) Bright field images showing otic region in 120-hour old injected control and (lower panel) otoferlin b+a double KDs, open arrow heads points to the otoliths, filled arrow heads point to the semicircular canals, white circle and hemicircle indicates position of the eye.

Figure 8 - **Rescue of zebrafish otoferlin knockdown with mouse otoferlin. A)** Schematic of the truncated mouse otoferlin constructs used in this study. Amino acid numbers are indicated. **B)** Whole mount immunohistochemistry on 120 hpf larval zebrafish double morphants co-injected with the mouse full-length otoferlin construct under the hair cell specific promoter. Figure shows otoferlin expression only in the hair cells at 120 hpf. **C)** Otoferlin deficiency causes defects in startle escape response in 120 hpf larval zebrafish. Plot of distance after startling for different groups. Control

(n=23, mean distance 63.94 mm), Otoferlin b KD (n=18, mean distance = 66.03 mm), Otoferlin a KD (n = 17, mean distance = 66.79 mm), Otoferlin b+a KD (n = 16, mean distance = 22.92 mm), Rescue FL (n = 18, mean distance = 59.58 mm), Rescue ΔABC (n = 19, mean distance = 63.32 mm), Rescue ΔABCD (n = 25, mean distance = 53.94 mm), Rescue ΔABCDE (n = 23, mean distance = 52.00 mm), Rescue ΔBCDEF (n = 16, mean distance = 26.57 mm), Rescue mRNA (n = 17, mean distance = 65.55 mm),(Dunn's multiple comparison with standard 5% significance between otoferlin a+b KD and other groups, p-value<0.001). Error bars indicate 95% confidence interval of the sample mean. ns = not significant. **D)** Mean velocity (in mm/ sec) traces of different groups - Control (n = 23), Otoferlin b+a KD (n = 16), Rescue FL (n = 18), Rescue ΔABC (n = 19). The time point of startle is denoted with a vertical arrow, and the first 10 secs after startling is denoted with a capped line.

Figure 9 - Rescue of otoferlin KD swim bladder phenotype with mouse otoferlin constructs. **A)** Rescue of swim bladder defect in 120 hpf otoferlin b+a KDs with FL-otoferlin. **B)** Rescue of swim bladder defect in 120 hpf otoferlin b+a KDs with del-ABC construct. **C)** Rescue of swim bladder defect in 120-hpf old otoferlin b+a double KD zebrafish with otoferlin mRNA. Arrow indicates inflated swim bladder. **D)** Table showing percentage of fish rescued at 120 hpf co-injected with mouse otoferlin constructs including otoferlin mRNA. (FL = full length).

631 **Acknowledgements:** This work was supported by a Medical Research Foundation
632 (MRF) grant to CPJ, as well as Oregon State University, and NIH P30 000210 (RLT).
633 We thank Prof. Teresa Nicolson for providing us with the p5E-pmyo6b vector, Prof.
634 Christine Petit for providing us with mouse otoferlin cDNA, Veterinary Diagnostic Lab,
635 Oregon State University, OR, for help with the paraffin sections, Carrie Barton for help
636 with fish maintenance and embryo collection, Mike T. Simonich for assembling the
637 startle apparatus, Kai Tao and Anne-Marie Girard for help with confocal microscopy,
638 Siba R. Das for advice on the Noldus software, Sean M. Bugel for advice on molecular
639 biology, Pamela Noyes for advice on Graphapad software, Leah Wehmas for advice on
640 agar block preparation, Jacob Thomas Huegel for help with co-localization images,
641 Justin Sanders for advice on in situ hybridization on zebrafish paraffin sections, Ananda
642 S. Roy for help with R-program.

643

644

645

646

647

648

649

650

References:

1. **Abdullah N, Padmanarayana M, Marty NJ, Johnson CP.** 2014. Quantitation of the calcium and membrane binding properties of the C2 domains of dysferlin. Biophys. J. **106:**382-389.
2. **Beurg M, Michalski N, Safieddine S, Bouleau Y, Schneggenburger R, Chapman ER, Petit C, Dulon D.** 2010. Control of exocytosis by synaptotagmins and otoferlin in auditory hair cells. J. Neurosci. **30:**13281-13290.
3. **Burgess HA, Granato M.** 2007. Sensorimotor gating in larval zebrafish. J. Neurosci. **27:**4984-4994.
4. **Dulon D, Safieddine S, Jones SM, Petit C.** 2009. Otoferlin Is Critical for a Highly Sensitive and Linear Calcium-Dependent Exocytosis at Vestibular Hair Cell Ribbon Synapses. J. Neurosci. **29:**10474-10487.
5. **Duncker SV, Franz C, Kuhn S, Schulte U, Campanelli D, Brandt N, Hirt B, Fakler B, Blin N, Ruth P, Engel J, Marcotti W, Zimmermann U, Knipper M.** 2013. Otoferlin couples to clathrin-mediated endocytosis in mature cochlear inner hair cells. J. Neurosci **33:**9508-9519.
6. **Faber DS, Fetcho JR, Korn H.** 1989. Neuronal networks underlying the escape response in goldfish. General implications for motor control. Ann. N. Y. Acad. Sci. **563:**11-33.
7. **Fuchs PA.** 2005. Time and intensity coding at the hair cell's ribbon synapse. J. Physiol-London. **566:**7-12.
8. **Goodyear RJ, Legan PK, Christiansen JR, Xia B, Korchagina J, Gale JE, Warchol ME, Corwin JT, Richardson GP.** 2010. Identification of the hair cell soma-1 antigen, HCS-1, as otoferlin. J. Assoc. Res. Otolaryngol. **11:**573-586.
9. **Griesinger CB, Richards CD, Ashmore JF.** 2002. Fm1-43 reveals membrane recycling in adult inner hair cells of the mammalian cochlea. J. Neurosci. **22:**3939-3952.
10. **He S, Yang J.** 2011. Maturation of neurotransmission in the developing rat cochlea: immunohistochemical evidence from differential expression of synaptophysin and synaptobrevin 2. Eur. J. Histochem. **55:**1-9.
11. **Heidrych P, Zimmermann U, Kuhn S, Franz C, Engel J, Duncker SV, Hirt B, Pusch CM, Ruth P, Pfister M, Marcotti W, Blin N, Knipper M.** 2009. Otoferlin interacts with myosin VI: implications for maintenance of the basolateral synaptic structure of the inner hair cell. Hum. Mol. Genet. **18:**2779-2790.
12. **Helfmann S, Neumann P, Tittmann K, Moser T, Ficner R, Reisinger E.** 2011. The crystal structure of the C(2)A domain of otoferlin reveals an unconventional top loop region. J. Mol. Biol. **406:**479-490.
13. **Howe K, Clark MD, Torroja CF, Torrance J, Berthelot C, Muffato M, Collins JE, Humphray S, McLaren K, Matthews L, McLaren S, Sealy I, Caccamo M, Churcher C, Scott C, Barrett JC, Koch R, Rauch GJ, White S, Chow W, Kilian B, Quintais LT, Guerra-Assuncao JA, Zhou Y, Gu Y, Yen J, Vogel JH, Eyre T, Redmond S, Banerjee R, Chi J, Fu B, Langley E, Maguire SF, Laird GK, Lloyd D, Kenyon E, Donaldson S, Sehra H, Almeida-King J, Loveland J, Trevanion S, Jones M, Quail M, Willey D, Hunt A, Burton J, Sims S, McLay K, Plumb B, Davis J, Clee C, Oliver K, Clark R, Riddle C, Elliot D,**

Threadgold G, Harden G, Ware D, Mortimore B, Kerry G, Heath P, Phillimore B, Tracey A, Corby N, Dunn M, Johnson C, Wood J, Clark S, Pelan S, Griffiths G, Smith M, Glithero R, Howden P, Barker N, Stevens C, Harley J, Holt K, Panagiotidis G, Lovell J, Beasley H, Henderson C, Gordon D, Auger K, Wright D, Collins J, Raisen C, Dyer L, Leung K, Robertson L, Ambridge K, Leongamornlert D, McGuire S, Gilderthorp R, Griffiths C, Manthravadi D, Nichol S, Barker G, Whitehead S, Kay M, Brown J, Murnane C, Gray E, Humphries M, Sycamore N, Barker D, Saunders D, Wallis J, Babbage A, Hammond S, Mashreghi-Mohammadi M, Barr L, Martin S, Wray P, Ellington A, Matthews N, Ellwood M, Woodmansey R, Clark G, Cooper J, Tromans A, Grafham D, Skuce C, Pandian R, Andrews R, Harrison E, Kimberley A, Garnett J, Fosker N, Hall R, Garner P, Kelly D, Bird C, Palmer S, Gehring I, Berger A, Dooley CM, Ersan-Urun Z, Eser C, Geiger H, Geisler M, Karotki L, Kirn A, Konantz J, Konantz M, Oberlander M, Rudolph-Geiger S, Teucke M, Osoegawa K, Zhu B, Rapp A, Widaa S, Langford C, Yang F, Carter NP, Harrow J, Ning Z, Herrero J, Searle SM, Enright A, Geisler R, Plasterk RH, Lee C, Westerfield M, de Jong PJ, Zon LI, Postlethwait JH, Nusslein-Volhard C, Hubbard TJ, Roest Crollius H, Rogers J, Stemple DL, Begum S, Lloyd C, Lanz C, Raddatz G, Schuster SC. 2013. The zebrafish reference genome sequence and its relationship to the human genome. Nature **496:**498-503.

14. **Javelle M, Marco CF, Timmermans M.** 2011. In situ hybridization for the precise localization of transcripts in plants. J. Vis. Exp. **57:**1-11
15. **Johnson CP, Chapman ER.** 2010. Otoferlin is a calcium sensor that directly regulates SNARE-mediated membrane fusion. J. Cell. Biol. **191:**187-197.
16. **Kappler JA, Starr CJ, Chan DK, Kollmar R, Hudspeth AJ.** 2004. A nonsense mutation in the gene encoding a zebrafish myosin VI isoform causes defects in hair-cell mechanotransduction. Proc. Natl. Acad. Sci. USA **101:**13056-13061.
17. **Khan Z, Carey J, Park HJ, Lehar M, Lasker D, Jinnah HA.** 2004. Abnormal motor behavior and vestibular dysfunction in the stargazer mouse mutant. Neuroscience **127:**785-796.
18. **Khimich D, Nouvian R, Pujol R, Tom Dieck S, Egner A, Gundelfinger ED, Moser T.** 2005. Hair cell synaptic ribbons are essential for synchronous auditory signalling. Nature **434:**889-894.
19. **Kimmel CB, Ballard WW, Kimmel SR, Ullmann B, Schilling TF.** 1995. Stages of embryonic development of the zebrafish. Dev. Dyn. **203:**253-310.
20. **Leibovici M, Safieddine S, Petit C.** 2008. Mouse models for human hereditary deafness. Curr. Top. Dev. Biol. **84:**385-429.
21. **LeMasurier M, Gillespie PG.** 2005. Hair-cell mechanotransduction and cochlear amplification. Neuron **48:**403-415.
22. **Lindema S, Gernet M, Bennay M, Koch M, Loscher W.** 2008. Comparative analysis of anxiety-like behaviors and sensorimotor functions in two rat mutants, ci2 and ci3, with lateralized rotational behavior. Physiol. Behav. **93:**417-426.
23. **Longo-Guess C, Gagnon LH, Bergstrom DE, Johnson KR.** 2007. A missense mutation in the conserved C2B domain of otoferlin causes deafness in a new mouse model of DFNB9. Hearing research **234:**21-28.

24. **Marty NJ, Holman CL, Abdullah N, Johnson CP.** 2013. The C2 domains of otoferlin, dysferlin, and myoferlin alter the packing of lipid bilayers. Biochemistry **52:**5585-5592.
25. **Mcmahon HT, Missler M, Li C, Sudhof TC.** 1995. Complexins - Cytosolic Proteins That Regulate Snap Receptor Function. Cell **83:**111-119.
26. **Mirghomizadeh F, Pfister M, Apaydin F, Petit C, Kupka S, Pusch CM, Zenner HP, Blin N.** 2002. Substitutions in the conserved C2C domain of otoferlin cause DFNB9, a form of nonsyndromic autosomal recessive deafness. Neurobiology of disease **10:**157-164.
27. **Nicolson T, Rusch A, Friedrich RW, Granato M, Ruppersberg JP, Nusslein-Volhard C.** 1998. Genetic analysis of vertebrate sensory hair cell mechanosensation: the zebrafish circler mutants. Neuron **20:**271-283.
28. **Nouvian R, Beutner D, Parsons TD, Moser T.** 2006. Structure and function of the hair cell ribbon synapse. J. Membr. Biol. **209:**153-165.
29. **Novak AE, Ribera AB.** 2003. Immunocytochemistry as a tool for zebrafish developmental neurobiology. Methods Cell Sci. **25:**79-83.
30. **Obholzer N, Wolfson S, Trapani JG, Mo W, Nechiporuk A, Busch-Nentwich E, Seiler C, Sidi S, Sollner C, Duncan RN, Boehland A, Nicolson T.** 2008. Vesicular glutamate transporter 3 is required for synaptic transmission in zebrafish hair cells. J. Neurosci. **28:**2110-2118.
31. **Pangrsic T, Lasarow L, Reuter K, Takago H, Schwander M, Riedel D, Frank T, Tarantino LM, Bailey JS, Strenzke N, Brose N, Muller U, Reisinger E, Moser T.** 2010. Hearing requires otoferlin-dependent efficient replenishment of synaptic vesicles in hair cells. Nat. Neurosci. **13:**869-876.
32. **Ramakrishnan NA, Drescher MJ, Drescher DG.** 2009. Direct interaction of otoferlin with syntaxin 1A, SNAP-25, and the L-type voltage-gated calcium channel Cav1.3. J. Biol. Chem. **284:**1364-1372.
33. **Ramakrishnan NA, Drescher MJ, Morley BJ, Kelley PM, Drescher DG.** 2014. Calcium Regulates Molecular Interactions of Otoferlin with SNARE Proteins Required for Hair Cell Exocytosis. J. Biol. Chem. **289(13):** 8750-66.
34. **Reim K, Mansour M, Varoqueaux F, McMahon HT, Sudhof TC, Brose N, Rosenmund C.** 2001. Complexins regulate a late step in Ca2+-dependent neurotransmitter release. Cell **104:**71-81.
35. **Reim K, Wegmeyer H, Brandstatter JH, Xue MS, Rosenmund C, Dresbach T, Hofmann K, Brose N.** 2005. Structurally and functionally unique complexins at retinal ribbon synapses. J. Cell Biol. **169:**669-680.
36. **Reisinger E, Bresee C, Neef J, Nair R, Reuter K, Bulankina A, Nouvian R, Koch M, Buckers J, Kastrup L, Roux I, Petit C, Hell SW, Brose N, Rhee JS, Kugler S, Brigande JV, Moser T.** 2011. Probing the functional equivalence of otoferlin and synaptotagmin 1 in exocytosis. J. Neurosci **31:**4886-4895.
37. **Rodriguez-Ballesteros M, Reynoso R, Olarte M, Villamar M, Morera C, Santarelli R, Arslan E, Meda C, Curet C, Volter C, Sainz-Quevedo M, Castorina P, Ambrosetti U, Berrettini S, Frei K, Tedin S, Smith J, Cruz Tapia M, Cavalle L, Gelvez N, Primignani P, Gomez-Rosas E, Martin M, Moreno-Pelayo MA, Tamayo M, Moreno-Barral J, Moreno F, del Castillo I.** 2008. A multicenter study on the prevalence and spectrum of mutations in the otoferlin

gene (OTOF) in subjects with nonsyndromic hearing impairment and auditory neuropathy. Hum. Mutat. **29:**823-831.

38. **Roux I, Hosie S, Johnson SL, Bahloul A, Cayet N, Nouaille S, Kros CJ, Petit C, Safieddine S.** 2009. Myosin VI is required for the proper maturation and function of inner hair cell ribbon synapses. Hum. Mol. Genet. **18:**4615-4628.

39. **Roux I, Safieddine S, Nouvian R, Grati M, Simmler MC, Bahloul A, Perfettini I, Le Gall M, Rostaing P, Hamard G, Triller A, Avan P, Moser T, Petit C.** 2006. Otoferlin, defective in a human deafness form, is essential for exocytosis at the auditory ribbon synapse. Cell **127:**277-289.

40. **Sabaliauskas NA, Foutz CA, Mest JR, Budgeon LR, Sidor AT, Gershenson JA, Joshi SB, Cheng KC.** 2006. High-throughput zebrafish histology. Methods **39:**246-254.

41. **Schug N, Braig C, Zimmermann U, Engel J, Winter H, Ruth P, Blin N, Pfister M, Kalbacher H, Knipper M.** 2006. Differential expression of otoferlin in brain, vestibular system, immature and mature cochlea of the rat. Eur. J. Neurosci. **24:**3372-3380.

42. **Schwander M, Sczaniecka A, Grillet N, Bailey JS, Avenarius M, Najmabadi H, Steffy BM, Federe GC, Lagler EA, Banan R, Hice R, Grabowski-Boase L, Keithley EM, Ryan AF, Housley GD, Wiltshire T, Smith RJH, Tarantino LM, Muller U.** 2007. A forward genetics screen in mice identifies recessive deafness traits and reveals that pejvakin is essential for outer hair cell function. J. Neurosci. **27:**2163-2175.

43. **Strenzke N, Chanda S, Kopp-Scheinpflug C, Khimich D, Reim K, Bulankina AV, Neef A, Wolf F, Brose N, Xu-Friedman MA, Moser T.** 2009. Complexin-I Is Required for High-Fidelity Transmission at the Endbulb of Held Auditory Synapse. J. Neurosci. **29:**7991-8004.

44. **Therrien C, Di Fulvio S, Pickles S, Sinnreich M.** 2009. Characterization of lipid binding specificities of dysferlin C2 domains reveals novel interactions with phosphoinositides. Biochemistry **48:**2377-2384.

45. **Thisse C, Thisse B.** 2008. High-resolution in situ hybridization to whole-mount zebrafish embryos. Nat. Protoc. **3:**59-69.

46. **Uthaiah RC, Hudspeth AJ.** 2010. Molecular anatomy of the hair cell's ribbon synapse. J. Neurosci **30:**12387-12399.

47. **Valiyaveettil M, Alamneh Y, Miller SA, Hammamieh R, Wang Y, Arun P, Wei Y, Oguntayo S, Nambiar MP.** 2012. Preliminary studies on differential expression of auditory functional genes in the brain after repeated blast exposures. J. Rehabil. Res. Dev. **49:**1153-1162.

48. **Vincent PF, Bouleau Y, Safieddine S, Petit C, Dulon D.** 2014. Exocytotic machineries of vestibular type I and cochlear ribbon synapses display similar intrinsic otoferlin-dependent Ca2+ sensitivity but a different coupling to Ca2+ channels. J. Neurosci. **34:**10853-10869

49. **Waterman RE, Bell DH.** 1984. Epithelial fusion during early semicircular canal formation in the embryonic zebrafish, Brachydanio rerio. Anat. Rec. **210:**101-114.

50. **Westerfield M**. 2000. The zebrafish book. A guide for the laboratory use of zebrafish (Danio rerio). 4th ed., Univ. of Oregon Press, Eugene.

51. **Winata CL, Korzh S, Kondrychyn I, Zheng W, Korzh V, Gong Z.** 2009. Development of zebrafish swimbladder: The requirement of Hedgehog signaling in specification and organization of the three tissue layers. Dev. Biol. **331:**222-236.

52. **Wright S, Hwang Y, Oertel D.** 2014. Synaptic Transmission between End Bulbs of Held and Bushy Cells in the Cochlear Nucleus of Mice with a Mutation in Otoferlin. J. Neurophysiol jn 00522 02014.

53. **Yasunaga S, Grati M, Chardenoux S, Smith TN, Friedman TB, Lalwani AK, Wilcox ER, Petit C.** 2000. OTOF encodes multiple long and short isoforms: genetic evidence that the long ones underlie recessive deafness DFNB9. Am. J. Hum. Genet. **67:**591-600.

54. **Yasunaga S, Grati M, Cohen-Salmon M, El-Amraoui A, Mustapha M, Salem N, El-Zir E, Loiselet J, Petit C.** 1999. A mutation in OTOF, encoding otoferlin, a FER-1-like protein, causes DFNB9, a nonsyndromic form of deafness. Nat. Genet. **21:**363-369.

55. **Zak M, Bress A, Brandt N, Franz C, Ruth P, Pfister M, Knipper M, Blin N.** 2012. Ergic2, a brain specific interacting partner of Otoferlin. Cell. Physiol. Biochem. **29:**941-948.

56. **Zottoli SJ , Faber DS.** 2000. The Mauthner cell: what has it taught us?Neuroscie -ntist **6**: 26-38

A)

Species	Otoferlin C2 domains (% identity with human)					
	C2A	C2B	C2C	C2D	C2E	C2F
Mouse	91	100	100	100	98	98
Rat	92	100	100	99	98	98
Rabbit	95	99	99	99	100	-
Guinea-Pig	94	99	98	100	99	98
Frog	-	78	91	91	94	96
Zebrafish						
1)otoferlin a	-	91	89	83	88	94
2)otoferlin b	77	91	89	83	92	95

B)

Species	% identity with **human** otoferlin peptide sequence
Mouse	95
Rat	93
Rabbit	93
Guinea-Pig	94
Frog	79
Zebrafish	
1) otoferlin a	74
2) otoferlin b	76

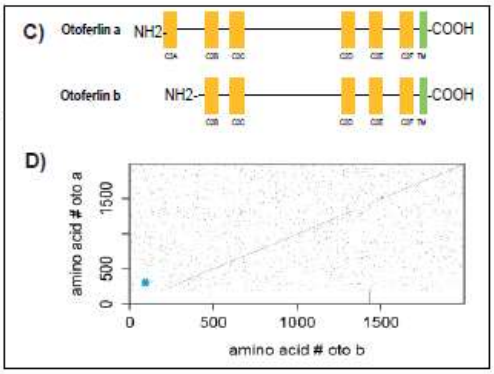

Figure 1 – Sequence identity of otoferlin across different species. **A)** Percent dentity of predicted otoferlin C2 domains of various species compared to human otoferlin. **B)** Comparison of overall sequence identity of otoferlin with human otoferlin. **C)** Zebrafish otoferlin isoforms with putative C2 domains. Otoferlin b lacks the C2A domain. **D)** Dot-plot showing the identity of amino acid sequence between the two zebrafish otoferlin proteins: otoferlin a and otoferlin b. The diagonal across the plot indicates highly identical sequnces. Breaks along the diagonal indicate regions which are non-identical. The asterisk (*) designates the absence of the C2A domain (amino acid = 3- 97).

856

857

858

859

860

861

862

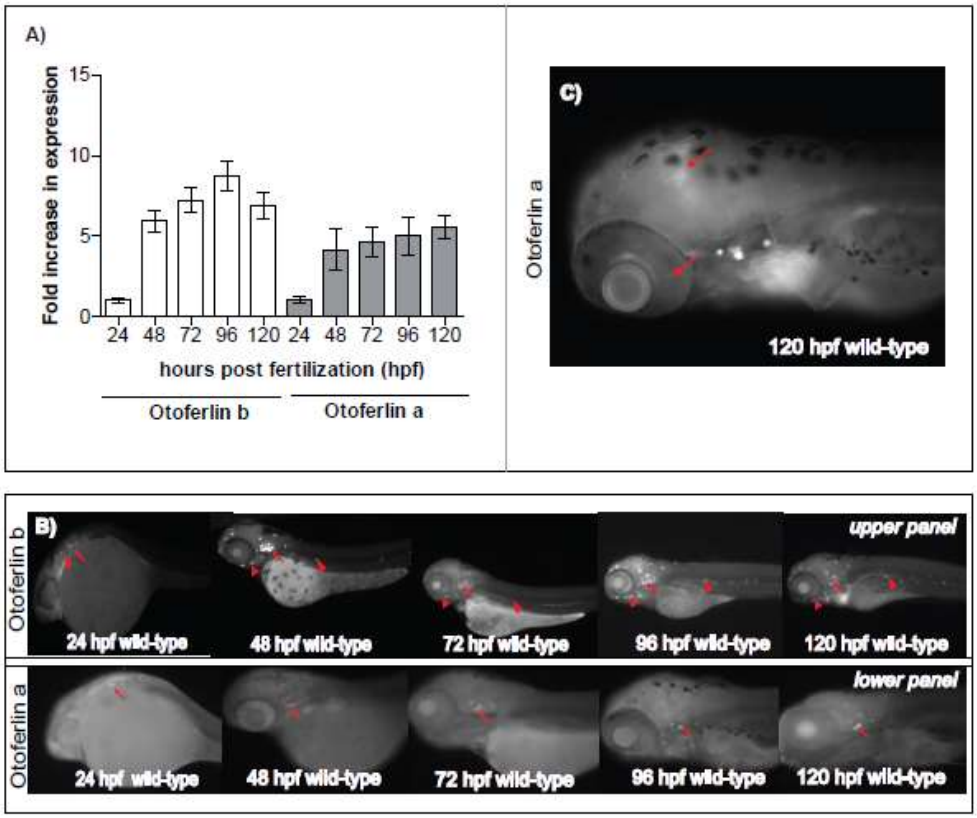

Figure 2 – mRNA expression of otoferlin in developing zebrafish. **A)** Fold expression of otoferlin a and b transcripts at 24-120 hpf. Expression is normalized to 24 hpf. Error bars indicate 95% confidence interval of the sample mean (n=5). **B)** Whole-mount in situ hybridization images showing expression of otoferlin in 24-120 hpf wild-type zebrafish larvae. Upper panel – Expression of otoferlin b. Arrows indicate sensory patches in the inner ear. Arrowheads indicate anterior and posterior lateral line neuromasts; Lower panel – Expression of otoferlin a. Arrows indicate sensory patches in the inner ear. **C)** Expression of otoferlin a in the brain region and retina in a 120 hpf zebrafish larvae. Arrows indicate brain and retina.

863

864

865

866

867

868

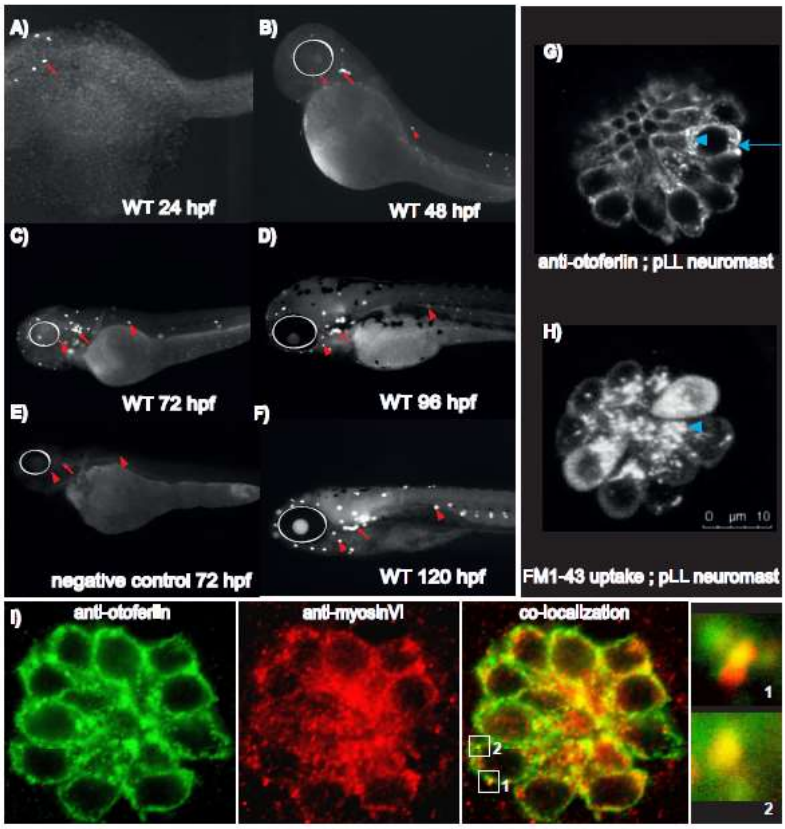

Figure 3 - Otoferlin protein expression in developing zebrafish. (**A-F**) Whole-mount immunohistochemistry on wild-type larval zebrafish at indicated developmental time points (24-120 hpf). **E)** Negative control with no primary antibody in 72 hpf wild-type larvae. White circles indicate the position of the eye, arrows indicate sensory patches of the ear, arrowheads denote anterior and lateral line neuromasts. **G)** Confocal image showing sub-cellular distribution of otoferlin in a 120 hpf hair cell neuromast cluster (Scalebar 10um). Arrowhead indicates the supranuclear region of the hair cell, arrow indicates basolateral compartment of the hair cell. **H)** Confocal image showing uptake of FM1-43 dye uptake in the apical end (arrowhead) of hair cells within a neuromast of the posterior lateral line. Dye incubation time – 3 minutes. **I)** Dual Immunofluorescence with wild-type 120 hpf zebrafish showing co-localization of otoferlin in the hair cells of the neuromast with another hair cell marker, myosinVI. White boxes 1 and 2 indicate regions of co-localization. Insets of regions 1 and 2 showing otoferlin co-localizing with myosinVI.

869

870

871

Molecular and Cellular Biology

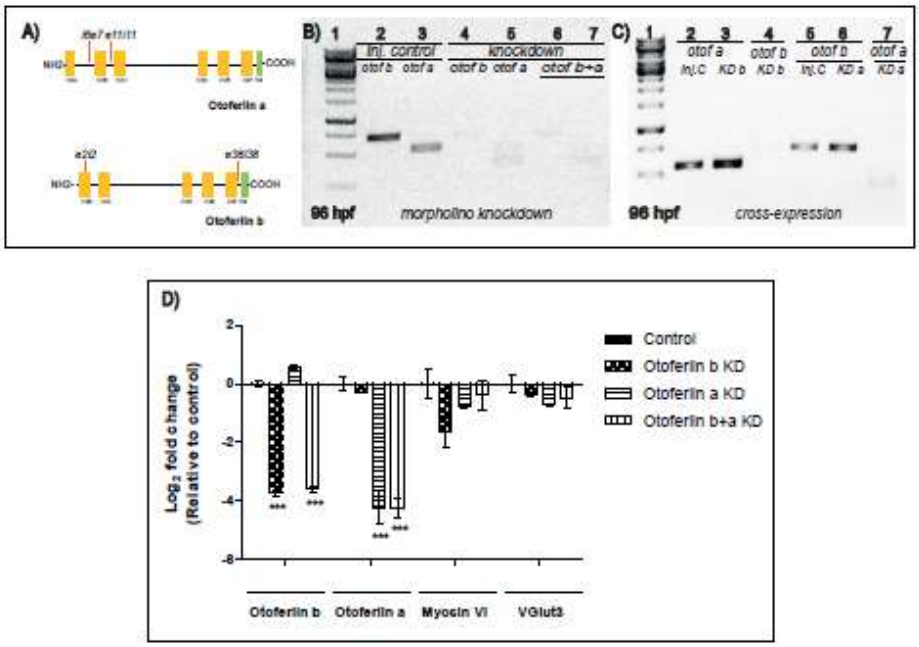

Figure 4 - Morpholino knockdown of otoferlin in zebrafish larvae. **A)** Diagram of four splice-blocking morpholinos used in this study targeting otoferlin a and otoferlin b (e= exon; i= intron). **B)** RT-PCR gel image of otoferlin KD zebrafish larvae at 96 hpf, (lane 1) = molecular weight marker ; (lane 2) = negative control tested for otoferlin b; (lane 3) = negative control injected tested for otoferlin a; (lane 4)= otoferlin b KD tested for otoferlin b; (lane 5) = otoferlin a KD tested for otoferlin a; (lane 6) = otoferlin b+a double KD tested for otoferlin b; (lane 7) = otoferlin b+a double KD tested for otoferlin a. **C)** Cross expression studies with 96 hpf zebrafish larvae. RT-PCR gel image shows expression of: (lane 1)= molecular weight marker; (lane 2) = otoferlin a in control; (lane 3)= otoferlin a in otoferlin b KD; (lane 4) = otoferlin b in otoferlin b KD; (lane 5) = otoferlin b in control; (lane 6)= otoferlin b in otoferlin a KD; (lane 7) = otoferlin a in otoferlin a KD. (Inj. C – injected control, KD – Knockdown, otof a – otoferlin a, otof b – otoferlin b, otof b+a – otoferlin b+a) **D)** qPCR bar graph showing relative expression of otoferlin a, otoferlin b, myosinVI and VGlut3 genes in 96 hpf larval zebrafish across control, otoferlin a KD, otoferlin b KD and otoferlin b+a KD groups where each gene is normalized with respect to the corresponding controls. For the Myosin VI and Vglut3 genes, no statistical deviation in expression is observed among the different KD groups. Expression of otoferlin a is significantly reduced (p value <0.001) in the otoferlin a and otoferlin b+a KD groups, but not in the otoferlin b KD. Otoferlin b expression is significantly reduced in the otoferlin b and otoferlin b+a KD groups (p value <0.001), but not in the otoferlin a KD. The statistical significance is calculated through Bonferroni multiple comparisons in prism software. Error bars indicate 95% confidence interval of the sample mean (n=3).

872

873

874

Molecular and Cellular Biology

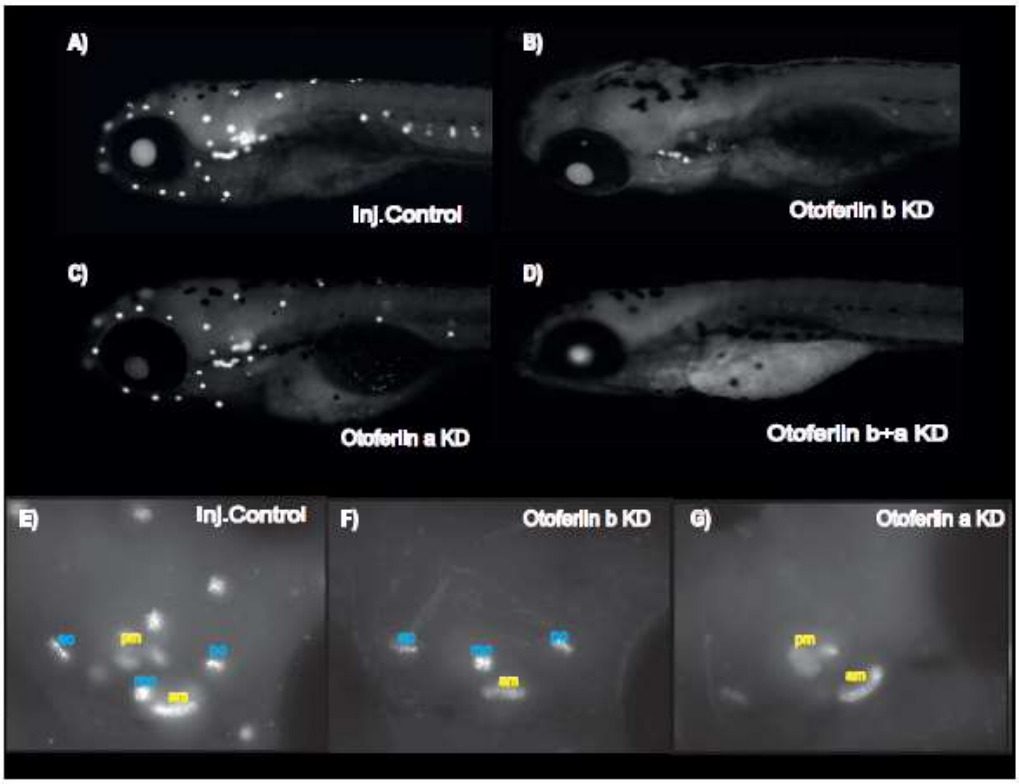

Figure 5 - Whole mount immunohistochemistry with the HCS-1 anti-otoferlin antibody. **A)** 120 hpf larvae showing otoferlin expression in control injected, **B)** otoferlin b KD, **C)** otoferlin a KD, **D)** otoferlin b+a KD. Fluorescent MIP (maximum intensity projection) image of **E)** Injected Control, **F)** Otoferlin b KD, **G)** Otoferlin a KD, of 120 hpf larval otic region showing distinct distribution of otoferlin in the sensory patches of cristae and maculae (ac, anterior crista; mc, medial crista; pc, posterior crista; pm, posterior macula; am, anterior macula).

875

876

877

878

879

880

881

882

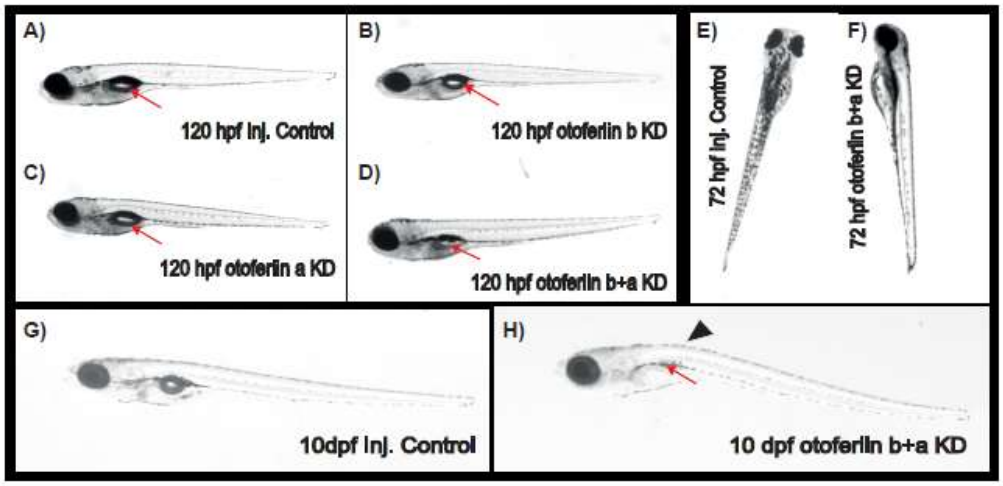

Figure 6 - Observable phenotypes associated with the otoferlin KD 120 hpf larval zebrafish. **A)** Control injected, **B)** otoferlin b KD, **C)** otoferlin a KD, **D)** otoferlin b+a double KD (arrows denote the swim bladder). The otoferlin double KDs fail to develop an inflated swim bladder. **E)** 72 hpf control larvae maintains an upright posture, **F)** 72 hpf otoferlin b+a double KDs fail to maintain an upright posture **G)** 10-day old injected control larvae, **H)** 10-day old otoferlin b+a double KD zebrafish fail to inflate their swim bladders (arrow) and develops a curved spine (arrow-head).

883

884

885

886

887

888

889

890

891

892

893

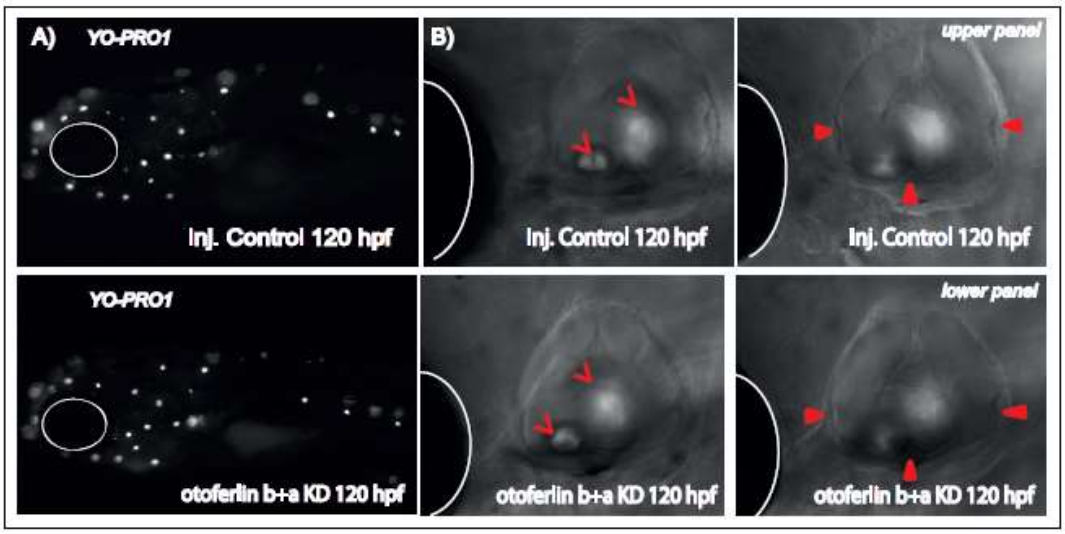

Figure 7 - Otoferlin KD effect on structure and formation of lateral line, otic vesicle and semi-circular canals. **A)** (upper panel) Yo-Pro1 uptake in injected control larval zebrafish at 120 hpf, (lower panel) Yo-Pro1 uptake in otoferlin b+a double KD larval zebrafish at 120 hpf **B)** (upper panel) Bright field images showing otic region in 120-hour old injected control and (lower panel) otoferlin b+a double KDs, open arrow heads points to the otoliths, filled arrow heads point to the semicircular canals, white circle and hemicircle indicates position of the eye.

894

895

896

897

898

899

900

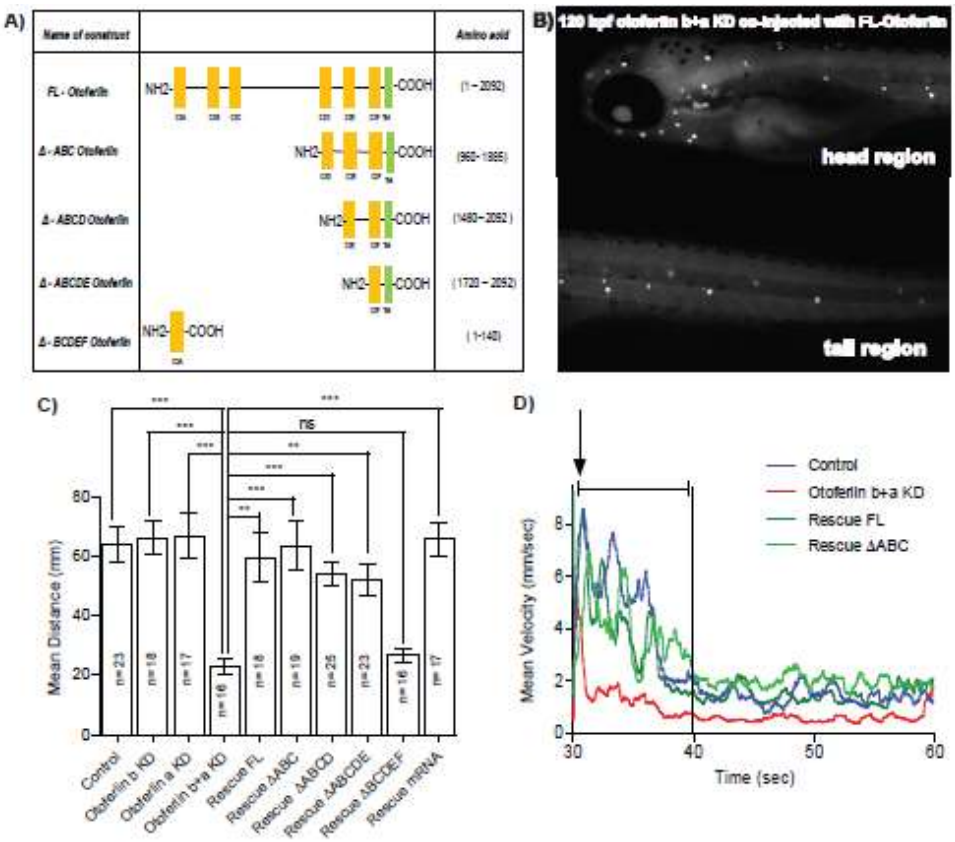

Figure 8 - Rescue of zebrafish otoferlin knockdown with mouse otoferlin. **A)** Schematic of the truncated mouse otoferlin constructs used in this study. Amino acid numbers are indicated. **B)** Whole mount immunohistochemistry on 120 hpf larval zebrafish double morphants co-injected with the mouse full-length otoferlin construct under the hair cell specific promoter. Figure shows otoferlin expression only in the hair cells at 120 hpf. **C)** Otoferlin deficiency causes defects in startle escape response in 120 hpf larval zebrafish. Plot of distance after startling for different groups. Control (n=23, mean distance 63.94 mm), Otoferlin b KD (n=18, mean distance = 66.03 mm), Otoferlin a KD (n = 17, mean distance = 66.79 mm), Otoferlin b+a KD (n = 16, mean distance = 22.92 mm), Rescue FL (n = 18, mean distance = 59.58 mm), Rescue ΔABC (n = 19, mean distance = 63.32 mm), Rescue ΔABCD (n = 25, mean distance = 53.94 mm), Rescue ΔABCDE (n = 23, mean distance = 52.00 mm), Rescue ΔBCDEF (n = 16, mean distance = 26.57 mm), Rescue mRNA (n = 17, mean distance = 65.55 mm),(Dunn's multiple comparison with standard 5% significance between otoferlin a+b KD and other groups, p-value<0.001). Error bars indicate 95% confidence interval of the sample mean. ns = not significant. **D)** Mean velocity (in mm/ sec) traces of different groups - Control (n = 23), Otoferlin b+a KD (n = 16), Rescue FL (n = 18), Rescue ΔABC (n = 19). The time point of startle is denoted with a vertical arrow, and the first 10 secs after startling is denoted with a capped line.

901

902

903

904

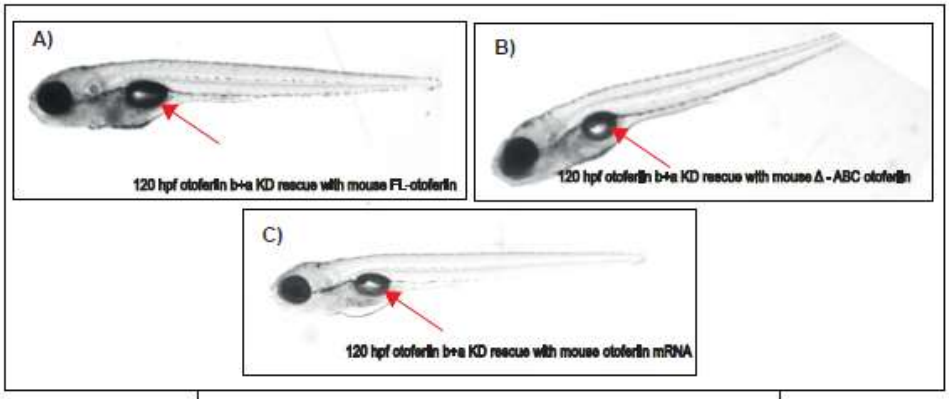

D) Otoferlin morphants co-injected with mouse rescue construct	Number of fish injected per group	% of injected larvae with inflated swim bladder
mRNA	120	22
FL-otoferlin	120	27
Δ-ABC	120	42
Δ-ABCD	150	16
Δ-ABCDE	110	20

Figure 9 - Rescue of otoferlin KD swim bladder phenotype with mouse otoferlin constructs. **A)** Rescue of swim bladder defect in 120 hpf otoferlin b+a KDs with FL-otoferlin. **B)** Rescue of swim bladder defect in 120 hpf otoferlin b+a KDs with del-ABC construct. **C)** Rescue of swim bladder defect in 120-hpf old otoferlin b+a double KD zebrafish with otoferlin mRNA. Arrow indicates inflated swim bladder. **D)** Table showing percentage of fish rescued at 120 hpf co-injected with mouse otoferlin constructs including otoferlin mRNA. (FL = full length).

905

906

907

908

909

910

911

912

913

914

915

916

917

Molecular and Cellular Biology